ACS APPLIED MATERIALS & INTERFACES

Research Article

www.acsami.org

Unexpected Enhancement in Antibacterial Activity of *N*-Halamine Polymers from Spheres to Fibers

Jing Kang,[†] Jinsong Han,[†] Yangyang Gao,[†] Tianyi Gao,[†] Shi Lan,[‡] Linghan Xiao,[§] Yanling Zhang,[†] Ge Gao,[⊥] Harnoode Chokto,[†] and Alideertu Dong*[,†]

[†]College of Chemistry and Chemical Engineering, Inner Mongolia University, Hohhot 010021, People's Republic of China

[‡]College of Science, Inner Mongolia Agricultural University, Hohhot 010018, People's Republic of China

[§]College of Chemistry and Life Science, Changchun University of Technology, Changchun 130012, People's Republic of China

[⊥]College of Chemistry, Jilin University, Changchun 130021, People's Republic of China

ABSTRACT: Preventing bacterial infections is a main focus of medical care. Antibacterial agents with broad and excellent disinfection capability against pathogenic bacteria are in fact urgently required. Herein, a novel strategy for the development of *N*-halamine polymers from spheres to fibers using a combined copolymerization-electrospinning-chlorination technique was reported, allowing fight against bacterial pathogen. Optimizing the process conditions, e.g., comonomer molar ratio, concentration of electrospinning solution, chlorination order, and chlorination period, resulted in the formation of *N*-halamine fibers with controllable morphology. *N*-Halamine polymers were tested against two common bacterial pathogens, *Escherichia coli* and *Staphylococcus aureus*, and were found to be extremely potent against both bacteria, suggesting that they possess powerful sterilizing properties. Remarkably, compared with those with sphere morphology, *N*-halamine fibers show unexpected enhancement toward both pathogens possibly because of their shape (fiber morphology), surface state (rough surfaces), and surface charge (positive zeta potentials). It is believed that this approach has great potential to be utilized in various fields where antifouling and antibacterial properties are highly required.

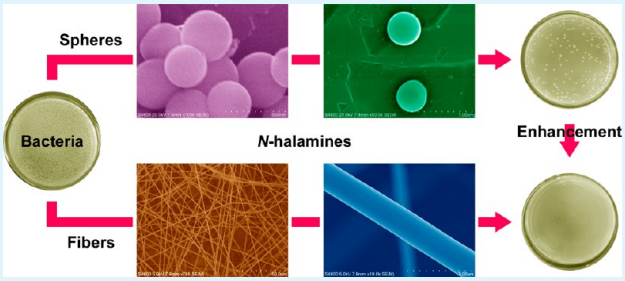

KEYWORDS: *N-halamine, fiber, sphere, antibacterial, enhancement*

INTRODUCTION

Microorganism threats on humans and ecosystems continue to be one of the greatest health challenges worldwide.[1] Microbial contamination induced by bacterial pathogen can cause various adverse effects on human safety.[2] Development of powerful antibiotics to control microbial contamination is, hence, urgently demanded. *N*-Halamines containing one or more nitrogen-halogen covalent bond in structure have become efficient tools for combating with pathogenic bacteria because of their almost instant and total sterilization of a wide range of microbes.[3] Notably, *N*-halamines are well-known for their unique features such as stability for a wide temperature and humidity range, durability over long-term usage, and regenerability upon exposure to washing cycles.[4−7] Therefore, *N*-halamines are applied in the fields of water purification systems, food storage and packaging, medical devices, hospital, hygienic products, dental office equipment, household sanitation, and so on.[8] As reported in our previous work, antibacterial performances of *N*-halamines strongly depend on their activated surface area.[9] Enlarging specific surface areas can enhance the sensitivity of such sterilization. To achieve this goal, we import electrospinning technique in this study to synthesize fibers for developing smaller sized *N*-halamines.

Electrospinning is an effective approach for fabricating various composite fibers.[10−17] Electrospun fibers with small sizes have a large specific surface area per unit mass, which has potential to provide unusually high sensitivity and fast response in sterilization application.[18] Fabricating *N*-halamine fibers with enlarged active surface area via electrospinning is intensely desirable. To date, electrospun *N*-halamine fibers serve as polymer biocides prepared via mixing cellulose acetate, polyacrylonitrile, or nylon-6 with *N*-halamine followed by electrospinning method have been reported.[19−21] Nevertheless, these *N*-halamines mixed physically with fibers suffer from annoying issues such as maldistribution, aggregation, and leakage. To tackle these problems, a more straightforward method is covalent grafting of *N*-halamines onto the surfaces of polymer fibers to introduce antibacterial functionalities permanently with a reasonably high effciency. Undesirably, it is much more difficult in forming *N*-halamine homopolymers with high molecular weight due to the radical autoinhibition of allylic structure of *N*-halamine monomer.[22] Nevertheless, *N*-halamines can form copolymers with many acrylic, substituted-

Received: June 18, 2015
Accepted: July 20, 2015
Published: July 20, 2015

DOI: 10.1021/acsami.5b05429
ACS Appl. Mater. Interfaces 2015, 7, 17516−17526

Scheme 1. (A–C) Formation Process and (D) Morphology Transformation of *N*-Halamine Fibers Using the Combined Copolymerization–Electrospinning–Chlorination Technique

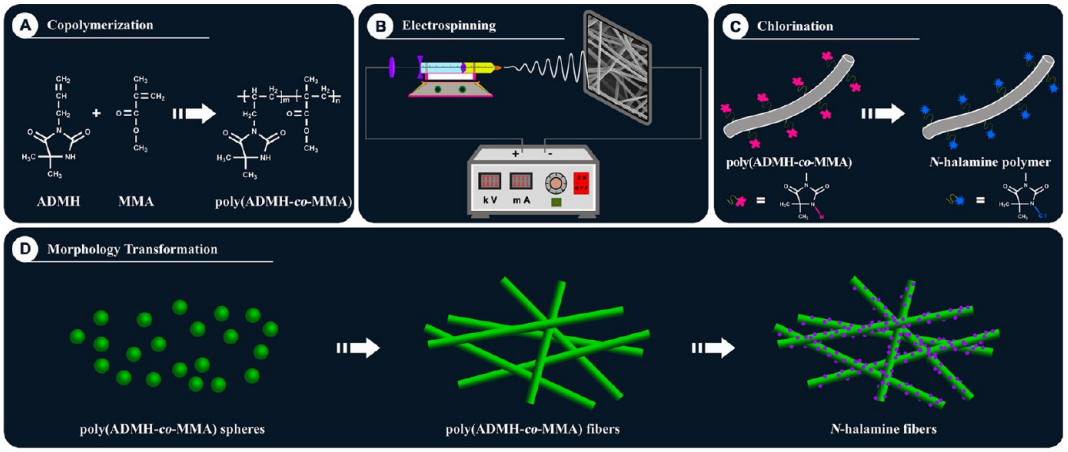

acrylic, and vinyl monomers in satisfactory yields.[22] Consequently, methyl methacrylate (MMA) was selected herein to copolymerize with *N*-halamine monomer to obtain *N*-halamine-modified poly(methyl methacrylate) (PMMA) because the ester group stabilize the radicals and simultaneously improve the reactivity of the monomer toward chain propagation reaction.[13] A major advantage of this copolymerization method is that by covalent grafting, *N*-halamine molecules could be rationally brought into the antibiotic system.

Inspired by these methods, we have successfully developed a strategy to construct novel antibiotic system, in which the *N*-halamine functionalized PMMA fibers are fabricated for the first time by the combined copolymerization-electrospinning-chlorination (CEC) technique (Scheme 1). We chose 3-allyl-5,5-dimethylhydantoin (ADMH) as *N*-halamine monomer to copolymerize with MMA first (Scheme 1A), and then synthesized hydantoin-modified PMMA fibers via electrospinning technique (Scheme 1B), and *N*-halamine fibers were finally obtained via the N–H → N–Cl transformation after chlorination process (Scheme 1C). Unexpectedly, thanks to the morphological transformation (Scheme 1D), *N*-halamine fibers exert enhanced toxicity toward bacteria compared with those with spherical *N*-halamines. It has been proven that the synergism of these three approaches can dramatically improve the bactericidal activity of *N*-halamine fibers utilized as an antibiotic to fight against bacterial pathogen. Unlike conventional *N*-halamines, the inherent features of the as-designed fibers with advantages of high sensitivity and fast response allow them to be potential as efficient antibacterial agents. Given that *N*-halamine fibers have excellent antibacterial activity, we believe that they could be widely applied in various fields such as medical devices, health care products, water purification systems, hospitals, dental office equipment, and food storage.

EXPERIMENTAL SECTION

Materials. Allyl bromide and 5,5-dimethylhydantoin (DMH) were purchased from Aladdin Industrial, Inc. Methyl methacrylate (MMA), methanol (MeOH), *N*,*N*-dimethylformamide (DMF), potassium hydrate (KOH), and potassium persulfate (KPS) were obtained from Tianjin Chemical Reagent Plant. Sodium hypochlorite (NaClO) was provided from Sinopharm Chemical Reagent Co., Ltd.

Synthesis of *N*-Halamine Fibers. The synthesis of *N*-halamines fibers was accomplished as follows. About 6.4 g of DMH was added into 50 mL of deionized water containing 2.8 g of KOH, and the mixture was stirred at room temperature for 1 h. A 20 mL methanol solution with 4.4 mL allyl bromide was added into the above reaction system, and the solution was stirred at 60 °C for 6 h to obtain the 3-allyl-5,5-dimethylhydantoin (ADMH). A mixture of 0.1 g ADMH dissolved in 3 mL MMA was added into 150 mL ultrapure water containing 0.1 g KPS, and the copolymerization was accomplished at 75 °C for 24 h under the condition of N_2 gas inlet. The as-prepared poly(ADMH-*co*-MMA) was added into DMF and stirred overnight to prepare electrospinning solution. A buret with an inserted copper rod to connect with high voltage of 20 kV was filled with the DMF solution mentioned above. Aluminum foil, as the counter electrode, was fixed with a distance of about 20 cm from the buret tip. Electrospinning was carried out at room temperature to obtain poly(ADMH-*co*-MMA) fibers. Then the as-prepared polymer fibers were immersed into sodium hypochlorite solution, and the chlorination was accomplished at room temperature to obtain *N*-halamine fibers.

Characterizations. Morphology and size of the samples were examined by scanning electron microscopy (SEM, Shimadzu SSX-550). The energy-dispersive X-ray spectroscopy (EDX) was performed during the SEM measurements. Fourier transform infrared spectrometry (FTIR) spectra were recorded by using a Thermo Nicolet (Woburn, MA) Avatar 370 FTIR spectrometer. ^{1}H NMR spectra were recorded on a Bruker AVANCEIII-500 NMR spectrometer in DMSO solution. The zeta potentials of the samples were measured using a Multifunctional Zeta PALS Potential and Particle Size Analyzer (Brookhaven Instruments Corporation).

Plate Counting Method. 50 μL of bacteria suspension [*Staphylococcus aureus* (ATCC 25923, Gram-positive bacteria) and *Escherichia coli* (ATCC 25922, Gram-negative bacteria)] with a concentration of 10^6 CFU/mL was mixed with the sample suspension and incubated under constant shaking (200 rpm). After that, the mixture was serially diluted, and 100 μL of each dilution was dispersed onto Luria–Bertani (LB) growth medium. Survival colonies on LB plates were counted after incubation at 37 °C for 24 h.

Inhibition Zone Study. Sample powder was grinded and added into a circular mold with a diameter of 1.0 cm, and then pressed using a tablet machine to prepare the sample disc. As for inhibition zone study, the sample disc was placed onto the surface of LB agar plate overlaid with 500 μL of 10^6 CFU/mL of *E. coli*. After incubation at 37 °C for 24 h, the inhibition zone around the sample disc was visible.

RESULTS AND DISCUSSION

Scheme 1 illustrates the fabrication procedure of *N*-halamine fibers by the aid of a combined copolymerization-electrospinning-chlorination (CEC) technique through three-step process. In Scheme 1A, poly(ADMH-*co*-MMA) spheres were

DOI: 10.1021/acsami.5b05429
ACS Appl. Mater. Interfaces 2015, 7, 17516–17526

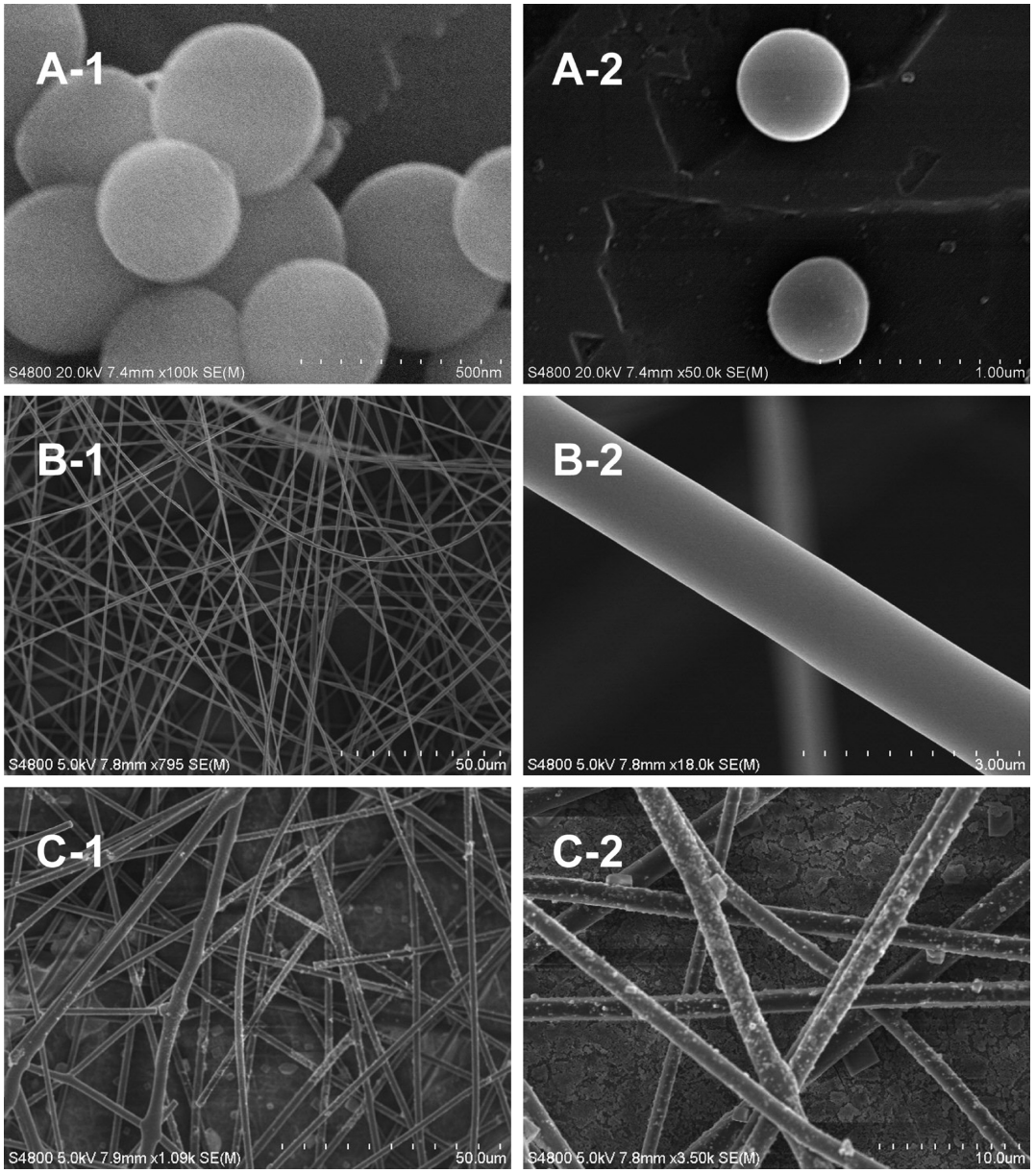

Figure 1. SEM images of (A-1 and A-2) poly(ADMH-*co*-MMA) spheres, (B-1 and B-2) poly(ADMH-*co*-MMA) fibers, (C-1 and C-2) *N*-halamine fibers.

facilely synthesized by a typical radical copolymerization. As reported, ADMH with amide N−H bond in structure is potent *N*-halamine precursor.[6] However, the allylic structure of ADMH can prevent its chain propagation reaction due to its autoinhibition behavior, and MMA can stabilize the radical and enhance the reactivity of the ADMH toward chain propagation reaction.[22] As a result, MMA was chosen to copolymerize with ADMH to form stable copolymer with sphere morphology. The as-synthesized poly(ADMH-*co*-MMA) polymers were dissolved in DMF at room temperature, and spheres were transformed to fibers using electrospinning procedure, as shown in Scheme 1B. After treatment with chlorine bleach, the N−H structure transformed to *N*-halamine, as shown in Scheme 1C. In this way, *N*-halamine polymer fibers were obtained skillfully from their corresponding sphere shape precursor (Scheme 1D) by a combined CEC approach.

Typical SEM images of the products were collected for the morphological understandings. In Figure 1A-1,A-2, poly(ADMH-*co*-MMA) shows quasi-monodisperse particles, spherical shapes, and smooth surfaces. Their sizes have a narrow range of 357.1−571.4 nm, and the mean particle size is 464.3 nm. After electrospinning, it can be seen in Figure 1B-1,B-2 that the images of poly(ADMH-*co*-MMA) is composed of numerous straight, randomly oriented fibers. Their surfaces do not display any serious cracks or irregularities. The average diameter is about 1.32 μm. It is obvious that the electrospinning can not only induce the morphology transformation but also drastically increase the size. After chlorination, the fibers become conglutinate, coarsened, tortuous slightly, but there is no significant change found in their sizes (Figure 1C-1,C-2), confirming that the chlorination treatment has no destructive effect on the polymer framework. More obviously in Figure 1C-2, some small white dots are detected on their surface, which further reflect N−H → N−Cl transformation. As proven, the activated surface area is one key parameter determining the biocidal efficiency of *N*-halamines.[23] These rough surfaces with

DOI: 10.1021/acsami.5b05429
ACS Appl. Mater. Interfaces 2015, 7, 17516−17526

small white dots scattered on fibers can act as the active sites for contacting and killing bacteria, as a result showing excellent antibacterial activity. These changes in morphology, size, and even surface state are effective evidence for the fabrication of *N*-halamine fibers.

Figure 2A,B show the patterns of EDS measurement of the poly(ADMH-*co*-MMA) fibers and *N*-halamine fibers. Peaks for

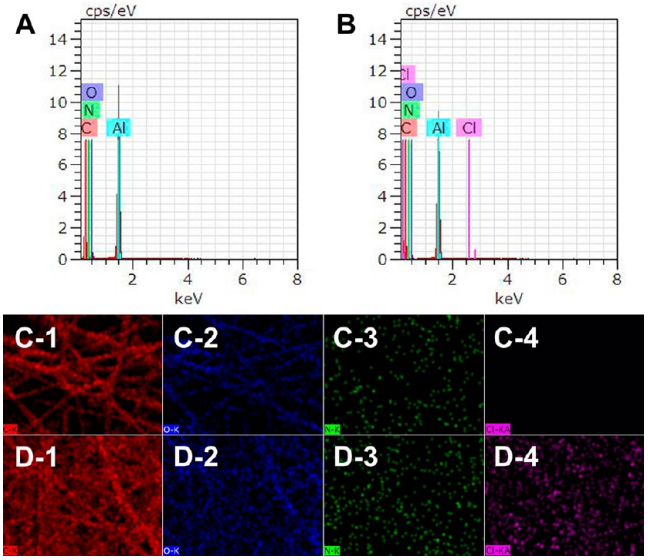

Figure 2. (A and B) EDS pattern and (C and D) elemental mapping of (A and C) poly(ADMH-*co*-MMA) fibers and (B and D) their corresponding *N*-halamine fibers.

the elements of C, O, and N are observed in Figure 2A, which match well with information for poly(ADMH-*co*-MMA) fibers. The intensive signal of elemental aluminum (Al) is from the substrate for the immobilization of electrospun fibers. Compared with poly(ADMH-*co*-MMA) fibers, the emergence of additional peaks for element Cl in Figure 2B confirms that the amide group of polymer was successfully transformed into the *N*-halamine structures. To further understand, we applied elemental mapping technique to ascertain the elemental distributions. The mapping results of poly(ADMH-*co*-MMA) and *N*-halamine fibers are illustrated in Figure 2C,D. In Figure 2C, elements C, O, N are observed, suggesting that ADMH was well copolymerized with MMA. In particular, the distributions of C and O dot signal are well matched and fiber-like appearances are detected, which is good agreement with SEM image in Figure 1B. The green dots of N element are desultorily distributed, implying that structural ADMH content is not as high as MMA in poly(ADMH-*co*-MMA) fibers. After bleaching treatment (Figure 2D), besides the dots for C, O, and N, fibers also show signal of element Cl scattered the whole image, which further confirms the success of N−H → N−Cl transformation.

To further confirm the fabrication of *N*-halamine, we performed FTIR spectroscopic analysis. Figure 3 exhibits the FTIR spectra of DMH, ADMH, MMA, poly(ADMH-*co*-MMA), and *N*-halamine fibers. They all exhibit bands attributed to methylene asymmetric C−H stretching and methylene symmetric C−H stretching.[24] Figure 3A shows C═O, C−N, and N−H characteristic peaks, confirming the structure of DMH molecules.[25] Beside these peaks, the additional peaks for C═C and ═C−H stretching vibration are clearly observed for ADMH (Figure 3B), which implies the success of allylation reaction.[26] MMA in Figure 3C shows the stretching vibration of C═O, C═C, ═C−H peaks.[27] Figure 3D remains most characteristic peaks mentioned above (C−H, C═O, C−N, and N−H), but the C═C and ═C−H stretching peak of ADMH (Figure 3B) and MMA (Figure 3C) monomers disappear, suggesting that ADMH and MMA were successfully copolymerized. Chlorinated product in Figure 3E presents almost the same characteristic spectrum with unchlorinated polymer in Figure 3D, except for the weakened N−H peak, which could be attributed to the *N*-halamine structure. The negligible weak N−H peak is likely attributed to the unchlorinated amide inside the fibers. These FTIR data indicate that the attachment of *N*-halamine onto PMMA fibers has indeed taken place via the combined CEC process.

The ^{1}H NMR spectrum was also recorded to further confirm that *N*-halamine fibers can be realized via the CEC technique (Figure 4). DMH shows two peaks in the region of 7.0−11.0, corresponding to the N-1 and N-3 protons, respectively, but in the ^{1}H NMR spectrum of ADMH, only one N−H band is

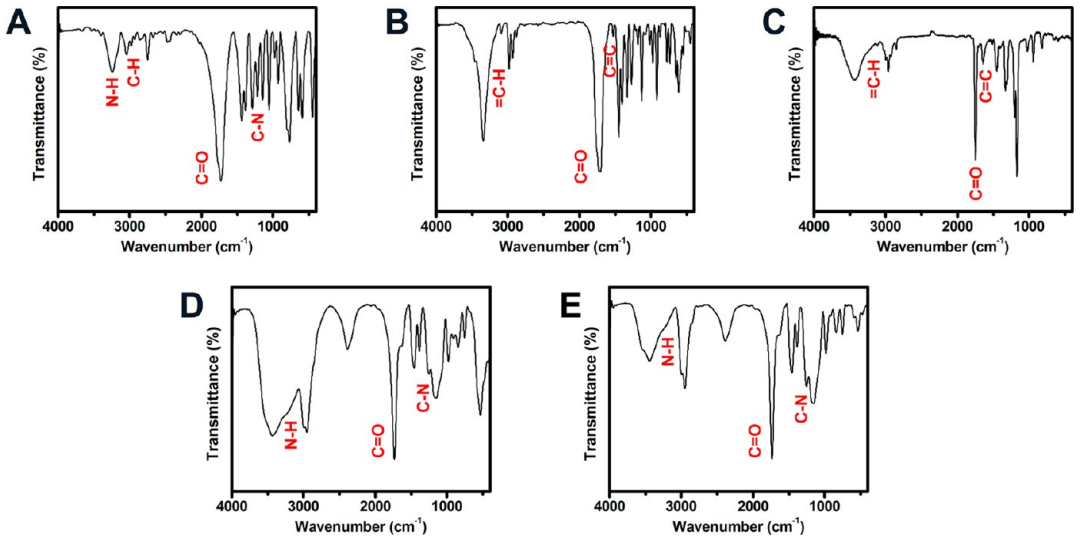

Figure 3. FTIR spectrum of (A) DMH, (B) ADMH, (C) MMA, (D) poly(ADMH-*co*-MMA), and (E) *N*-halamine.

DOI: 10.1021/acsami.5b05429
ACS Appl. Mater. Interfaces 2015, 7, 17516−17526

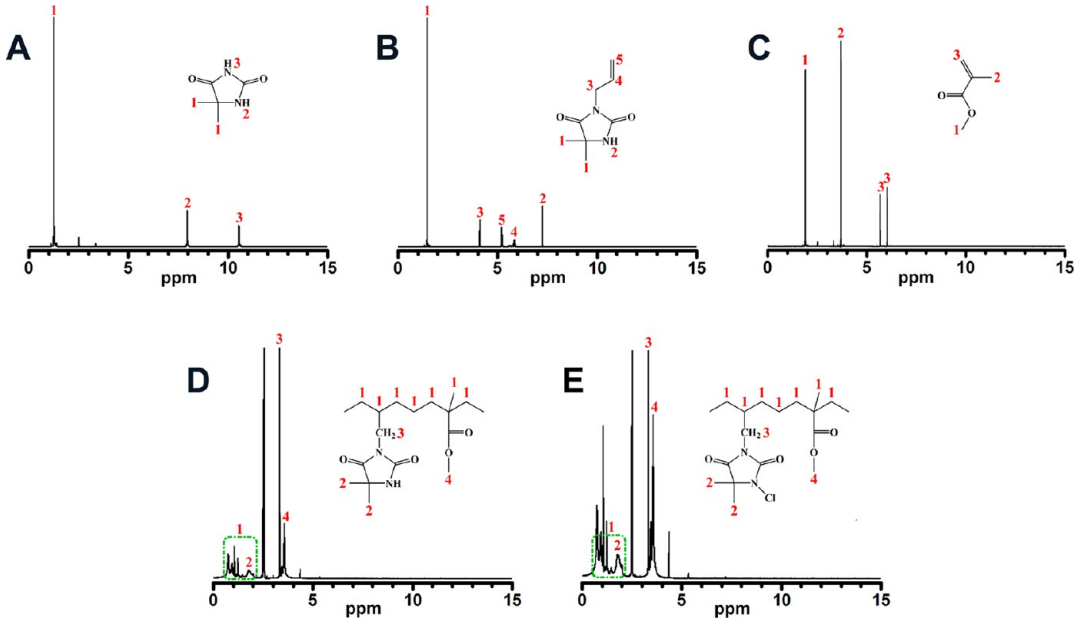

Figure 4. ^{1}H NMR of (A) DMH, (B) ADMH, (C) MMA, (D) poly(ADMH-*co*-MMA), and (E) *N*-halamines.

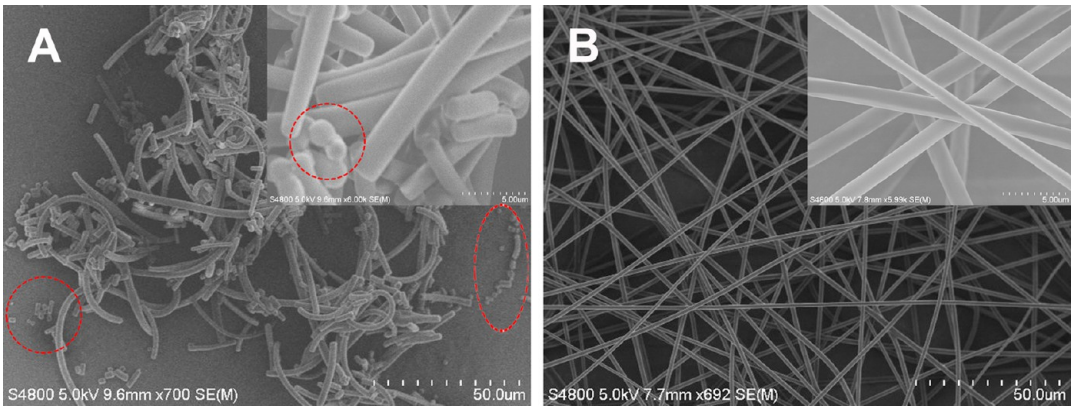

Figure 5. SEM image of poly(ADMH-*co*-MMA) fibers prepared at M_{ADMH}/M_{MMA} values of (A) 5/5 and (B) 1/9.

observed.[28] The disappearance of one proton is corresponding to the N-3 position substitution. Furthermore, the characteristic peaks of ADMH can be found at around 4.1 (N−CH_2), 5.8 (=CH−), and 5.2 (=CH_2), indicative of the allylic structure. These peaks prove the fact that N-3 proton of DMH was substituted by allylic structure. As for MMA, the =CH_2 group shows signals at 5.7 and 6.0 ppm, and the −CH_3 and O−CH_3 shows the resonance peak at 3.7 and 1.9 ppm, respectively.[29] After copolymerization, the characteristic CH, CH_2, and CH_3 signals are observed for poly(ADMH-*co*-MMA), while the CH_2= signals of ADMH and MMA component are no longer detected. The polymer shows obvious differences from their corresponding parent chemicals in ^{1}H NMR spectrum, which further confirms the formation of polymer. Upon chlorination, no significant is obtained except for the change in their intensities, which also reflects the transformation of the N−H → N−Cl.

During the preparation of poly(ADMH-*co*-MMA) via the radical copolymerization, molar ratio of ADMH to MMA (M_{ADMH}/M_{MMA}) plays a significant role in controlling ADMH content in copolymers. To clarify the fact, two different M_{ADMH}/M_{MMA} (5/5 and 1/9) values were utilized, while all other parameters were fixed. SEM images of poly(ADMH-*co*-MMA) fibers prepared at two different M_{ADMH}/M_{MMA} values are shown in Figure 5. The product with higher ADMH content (M_{ADMH}/M_{MMA} of 5/5) shows rod-like morphology but not fiber-like appearances (Figure 5A). Even some of them have length smaller than 1 μm (dotted line regions). Lower ADMH content product (M_{ADMH}/M_{MMA} of 1/9) in Figure 5B presents uniform straight fibers with narrow size distribution. More importantly, the diameters of these two products are different. These differences in morphology and size are further confirmed by the inset SEM images (Figure 5). Such differences in SEM images are possibly due to the reactivity difference between ADMH and MMA toward chain propagation reaction during the radical polymerization. ADMH can hardly provide high molecular weight polymers due to their allylic structures, while MMA has ester group and thus are favorable to radical polymerization.[22] It is difficult to obtain quite intact fibers via electrospinning technique using lower molecular weight polymer. As a result, introducing MMA herein to copolymerize with ADMH is the real reason for preparing high molecular weight polymer.

Electrospinning technique was found to be a unique and simple approach to synthesize fiber-based materials.[30] Concentration of electrospinning precursor solution is one key factor

DOI: 10.1021/acsami.5b05429
ACS Appl. Mater. Interfaces 2015, 7, 17516−17526

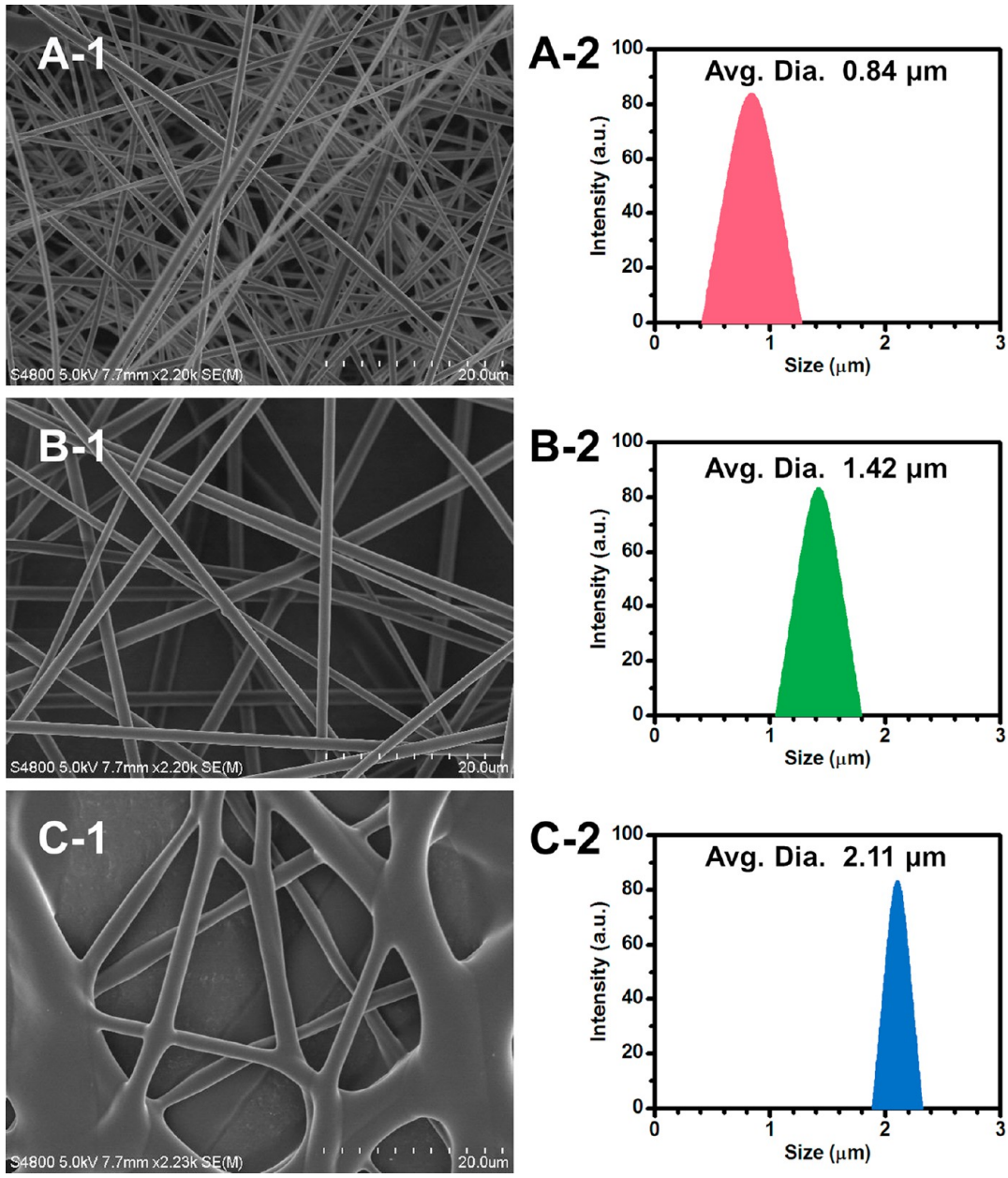

Figure 6. (Left) SEM images and (right) size distributions of poly(ADMH-*co*-MMA) fibers prepared at poly(ADMH-*co*-MMA) concentrations in DMF of (A) 9.1, (B) 12.7, and (C) 14.8 wt %.

for this technique. In this study, different poly(ADMH-*co*-MMA) concentrations (9.1, 12.7, and 14.8 wt %) in DMF were applied for the electrospinning experiment, and all the other parameters were kept constant. SEM images of the as-synthesized polymer fibers are shown in Figure 6 (left). At polymer concentration of 9.1 wt % (Figure 6A-1), quite straight and smooth fibers are detected. The corresponding size distribution was recorded and is given in Figure 6A-2. Their sizes range widely from 0.42 to 1.26 μm, and their average diameter is about 0.84 μm. When the concentration was increased to 12.7 wt % (Figure 6B-1), much thicker fibers are obtained. Their morphologies and surface states are almost the same as those at low concentration of 9.1 wt %. From Figure 6B-2, we find that the concentration of 12.7 wt % can provide a relative narrow size distribution (1.05−1.79 μm). The average diameter reaches as high as 1.42 μm. Further increasing polymer concentration to 14.8 wt % may lead to some assemblages as shown in Figure 6C-1. Although some fiber-like entities were clearly observed, there are more obvious for cross-linking among them. As a result, the integrity of the morphological fibers was destroyed. By determining the sizes for visible intact fibers from SEM images, the diameter distributions are in a quite narrow range of 1.89−2.32 μm. The most possible size is about 2.11 μm. In general, increasing concentration may be beneficial to controllable synthesis of narrow size fibers, whereas excessive high concentration may result in the fiber−fiber aggregation, as a result showing massive accumulation.

The oxidative chlorine content plays a decisive role in determining the antibacterial activity of *N*-halamines.[31] *N*-Halamines can always be synthesized by simple chlorination treatment.[31] To prove the effect of chlorination order on morphology, we chlorinated both spheres and fiber poly(ADMH-*co*-MMA) products, and their morphologies are

DOI: 10.1021/acsami.5b05429
ACS Appl. Mater. Interfaces 2015, 7, 17516−17526

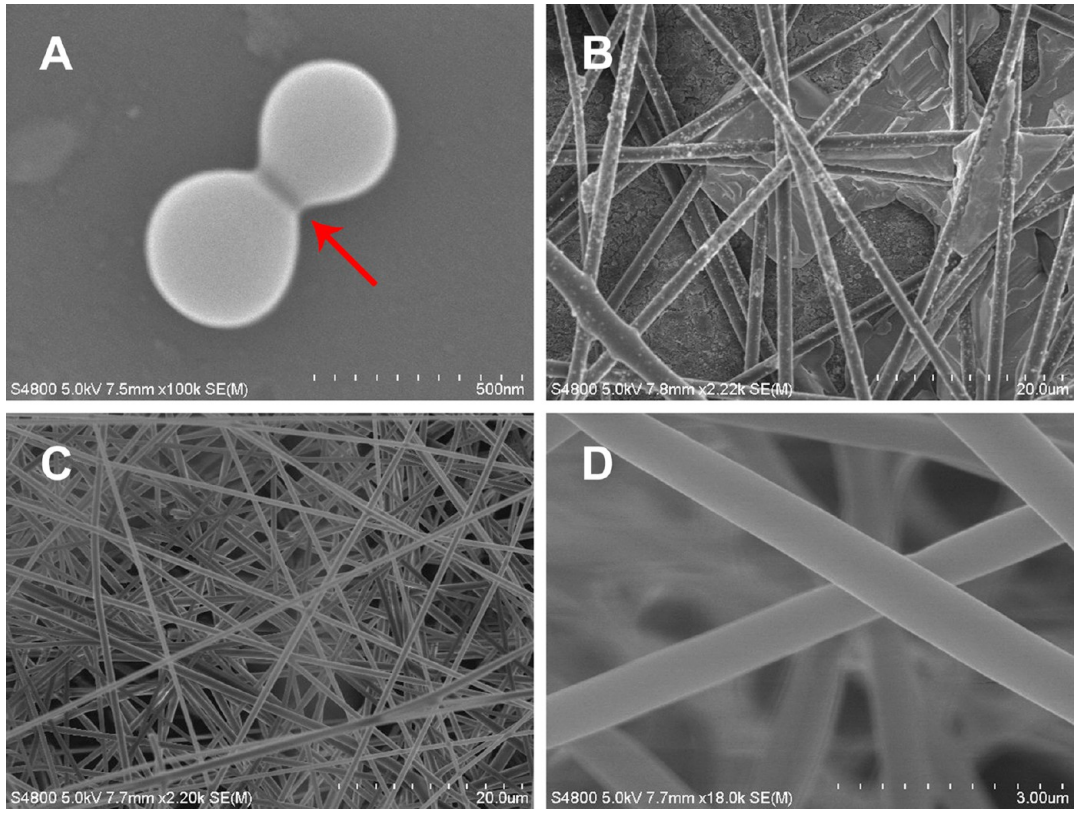

Figure 7. SEM image of *N*-halamine spheres and fibers prepared with different synthetic procedure: (A) copolymerization−chlorination (CC) technique, (B) copolymerization−electrospinning−chlorination (CEC) technique, and (C and D) copolymerization−chlorination−electrospinning (CCE) technique.

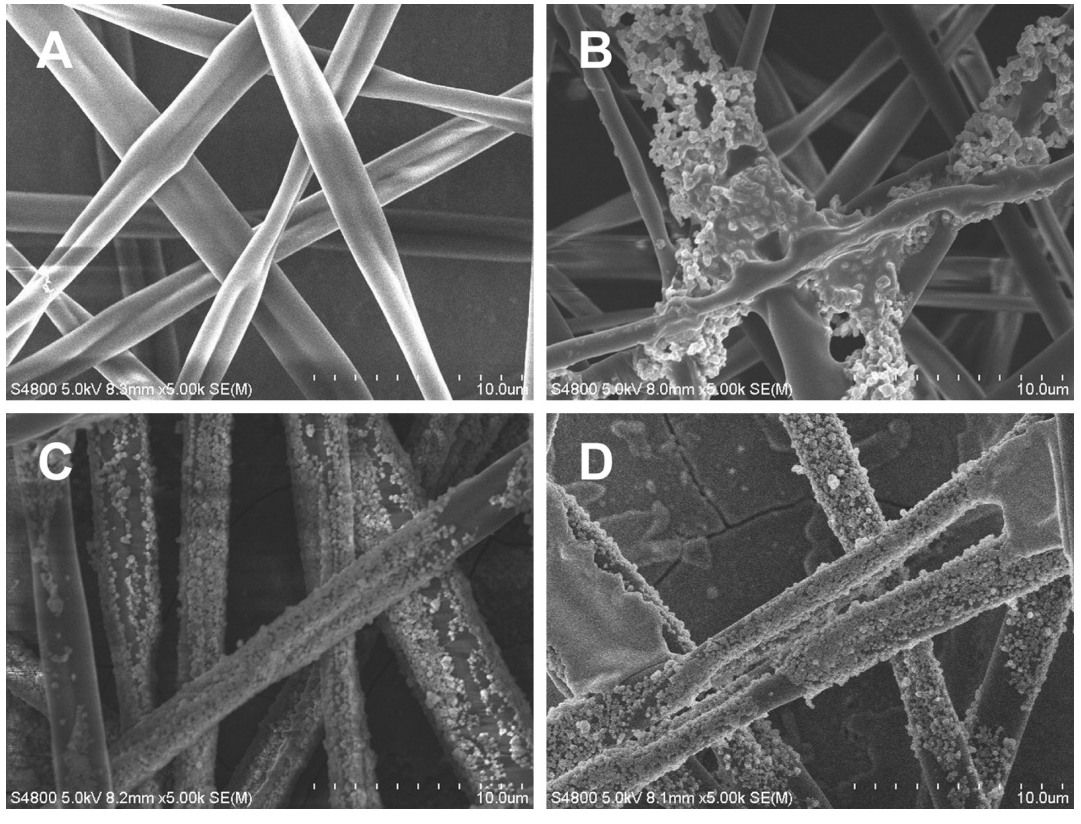

Figure 8. Effect of chlorination time on the morphology of *N*-halamine fibers: (A) 1, (B) 6, (C) 12, and (D) 24 h.

DOI: 10.1021/acsami.5b05429
ACS Appl. Mater. Interfaces 2015, 7, 17516−17526

illustrated in Figure 7A,B. Figure 7A is the SEM image of chlorinated products, which were prepared by the simple bleaching treatment of poly(ADMH-*co*-MMA) spheres. Like the untreated sample in Figure 1A-1,A-2, the as-prepared spheres show quite smooth surface. But cross-linking among spheres is detectable as underlined in Figure 7A. Such a morphology change can be one supplementary proof for N−H → N−Cl transformation. No significant change is found in their spherical shape and size, suggesting that the chlorine bleaching has almost no destructive effect on the polymer framework. The chlorinated fibers were also characterized by SEM as shown in Figure 7B. Their surfaces are decorated with small white dots, showing a thorn-like appearance. As for control, we also tried alternative route to prepare *N*-halamine fibers, that is, copolymerization−chlorination−electrospinning (CCE) technique. Interestingly, this approach produces quite smooth and perfect fibers (Figure 7C,D). We can hardly find any differences between these chlorinated fibers (Figure 7C,D) and poly(ADMH-*co*-MMA) fibers (Figure 1B-1,B-2). On the basis of these data, we can affirm that the chlorination order has significant effect on the morphology of the chlorinated polymers.

Enhancing active sites of *N*-halamines is one advisible route for improving their antibacterial capabilities.[32] To enhance active sites, we extended the chlorination time and evaluated the effect of chlorination time on the morphology of the chlorinated products. Chlorination times of 1, 6, 12, and 24 h were tested, and the corresponding SEM images are shown in Figure 8. Compared with gray colored fibers themselves, small white dots scattered on the surfaces of the fibers reflect the degree of the chlorination reaction. After 1 h of bleaching treatment (Figure 8A), the chlorinated fibers show almost the same morphology with unchlorinated sample (Figure 1B), which suggests that 1 h of chlorination is not enough for the N−H → N−Cl transformation. After a chlorination time of 6 h (Figure 8B), parts of the fibers are covered with small white dots, which can act as active sites for antibacterial performances. However, the dot coverage is fairly poor, and even some smooth fibers are visible, as shown in Figure 8B. When the chlorination reaction was carried out for 12 h (Figure 8C), the coverage is fairly dense and quite uniform. Further extending the bleaching time to 24 h (Figure 8D), uniform coverage is detectable, but some aggregations are observed. Such a developing trend suggests the controllable transformation of poly(ADMH-*co*-MMA) toward *N*-halamine by tuning bleaching period.

The antimicrobial activities of products were tested by the inhibition zone (DIZ) assay with *E. coli* and *S. aureus* as model bacteria (Figure 9).[33] DIZ value can represent the susceptibility of the bacteria toward the antibiotics.[34] For comparison, the pristine PMMA without *N*-halamine components was fabricated, and the corresponding DIZ value is illustrated as well. For both strains, PMMA disc has no inhibition zone around it, indicating that the support polymer is almost not toxic to bacteria. On the contrary, there are distinct aseptic halos around two chlorinated products. The spheres and fibers present obvious inhibition ring, which proves that both they have appreciable antibacterial capability both against *E. coli* and *S. aureus*. Therefore, it can be concluded that biocidal behavior of *N*-halamine-modified PMMA is based on the *N*-halamine structure other than PMMA support. As mentioned in our previous reports, *N*-halamines mainly contain two antibacterial mechanisms: contact killing and release killing.[35] The inhibition

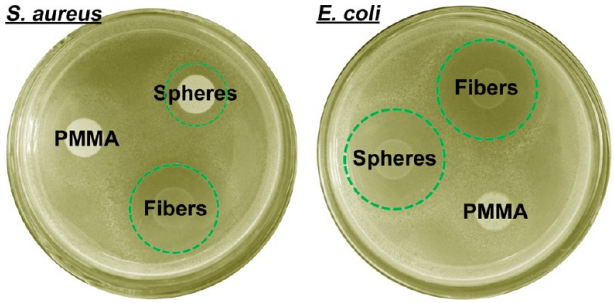

Figure 9. Inhibition zone assay for pure PMMA, *N*-halamine spheres, and *N*-halamine fibers against *S. aureus* and *E. coli*.

zone study herein gives some information about antibacterial mechanism for the release killing action of *N*-halamines. The release of oxidative chlorine induced by the dissociation of N−Cl structures is one significant explanation for the result of inhibition zone study.[35] The oxidative chlorine can release from the polymer support, killing bacteria as a result.

Because the effect of morphology on the antibacterial is not obvious from the inhibition zone test, we also carried out plate counting measurement.[36] The antibacterial activities of products with different morphologies were assayed via the LB agar culture plate with *E. coli* and *S. aureus* as models. Figure 10

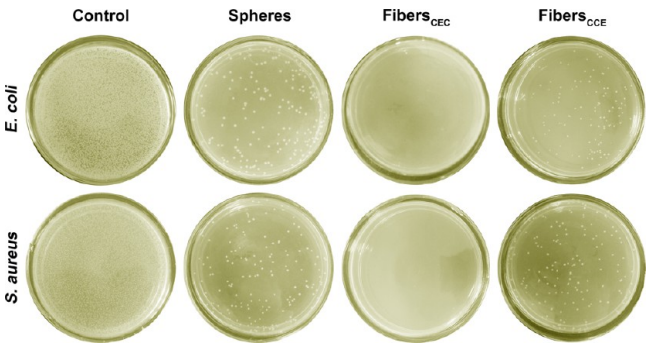

Figure 10. Photos showing the bacterial culture plates of *E. coli* and *S. aureus* upon 60 min exposure to the control, *N*-halamine spheres, *N*-halamine fibers$_{CEC}$, and *N*-halamine fibers$_{CCE}$.

shows the photographs of the plate counting method. The small white dots on LB agar plate are the survival bacterial colonies. On the control plate, both two bacteria present dense colonies, showing robust growth. Comparatively, the culture plates offer drastic decrease when they come into contact with *N*-halamines (spheres, fibers$_{CEC}$, and fibers$_{CCE}$), suggesting that all three products have excellent antimicrobial activities toward *E. coli* and *S. aureus*. As for sphere products, there are only several tens of colonies observed, implying that the sphere products can kill bacteria effectively. Compared with sphere products, fiber$_{CEC}$ products (prepared from CEC technique) display complete killings for both bacteria. Therefore, we can conclude that fibers$_{CEC}$ have higher antibacterial activity than spheres. Unlike the inhibition zone test, plate counting method gives different antibacterial capabilities for spheres and fibers. For comparison, fibers$_{CCE}$ (prepared via the CCE process) were also tested for antibacterial evaluation. The antibacterial results of fibers$_{CCE}$ are also shown in Figure 10. Some survival colonies are detectable for both strains, suggesting that the antibacterial capability of fibers$_{CCE}$ is not as high as fibers$_{CEC}$. The difference in the antibacterial performances between these two fibers

DOI: 10.1021/acsami.5b05429
ACS Appl. Mater. Interfaces 2015, 7, 17516−17526

might be explained by the difference in surface state. As presented in Figure 7B,C, although they offer similar fibrous morphology, $fibers_{CCE}$ (Figure 7C) displays a quite smooth surface and uniform size distribution, while $fibers_{CEC}$ (Figure 7B) gives a rough surface. Randomly located white dots on the surface of $fibers_{CEC}$ can be active sites for bacteria killing, offering enhanced antibacterial activity compared with $fibers_{CCE}$ with smooth surfaces as a result.

To further verify the morphology effect on antibacterial efficiency, we introduced sphere and fiber products to perform the time-kill assay. Time-kill assay is capable of observing the rate of the antibacterial extent.[37] *E. coli* was selected for time-kill assay. Figure 11A shows antibacterial results of the sphere and

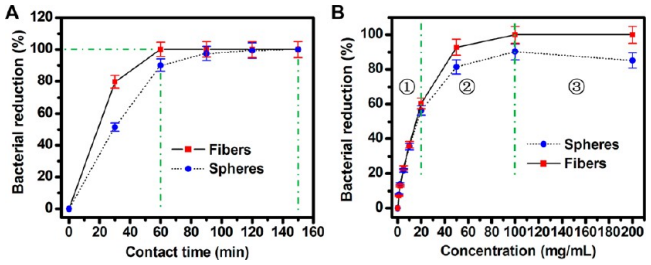

Figure 11. (A) Antibacterial time-kill assay graphs for *N*-halamines with different morphology (spheres and fibers) against *E. coli* as a function of contact time. (B) Effect of products concentration on the antibacterial activity of *N*-halamines with different morphology (spheres and fibers).

fiber products toward *E. coli* as a function of contact time within the range from 0 to 150 min. The bacterial reduction is calculated as % = $(B - A/B) \times 100$ (where A is the number of surviving bacterial colonies of the test sample, and B is that of the control).[38] As shown in Figure 11A, the number of surviving colonies decreases as the contact time increases. In general, two products give the similar tendency, that is, the bacterial reduction shows faster increasing speed first and then slows down with the aging time. Such a developing trend is in good agreement with those in our previous reports.[39] The time-kill assay also suggests morphology dependent manner against *E. coli*. It is clear that the antibiotic effects gradually change from a bacteriostatic to a bactericidal action with the morphology change from spheres to fibers. Through a detailed observation, sphere products inactivate about only 50% *E. coli* within 30 min, while fiber products show as high as about 80% killing at the same aging time. The bactericidal activity is fast-acting for fiber products, and their bactericidal end point is only 60 min, while sphere products have bactericidal end point of 150 min. Such an improvement in antibacterial activity induced by sphere-to-fiber transformation confirms the results of the plate counting method mentioned above (Figure 10). Therefore, it is quite evident that the morphology is one decisive factor for the antibiotic action. We inferred that the "effective" contact time is one possible reason for the enhanced antibacterial activity of fiber products compared with sphere products. The fiber products randomly dispersed in bacterial solution can act as "filter screen" and, as a result, increases the "effective" contact time of bacteria with the *N*-halamines to show improved antibacterial capability.

The concentration effect of the products on the antimicrobial activity was also evaluated by selecting *E. coli* as model microorganism. The concentrations are from 0 to 200 mg/mL, while other parameters are fixed. The antimicrobial experimental results of both sphere and fiber products are given in Figure 11B. Obviously, both two products show the similar trend, that is, the bacterial reduction rapidly rises at first and then levels off as the concentration further increases. The increase in bacterial reduction corresponds to the increase in concentration, which suggesting that the antibacterial activities of the products are in proportion to their concentrations. On a closer observation, there are some differences between these two products. When the concentration is lower than 20 mg/mL in region 1, the bacterial reduction of sphere products is almost the same as the fiber products. Namely, there is no significant difference between sphere and fiber products at lower concentration. Further extended concentration in region 2 shows relative differences between these two products. Fibers products display much more drastic promotion than sphere products. Fibers products with concentration of 100 mg/mL can give 100% bacteria killing, while the sphere products show about 90% bacterial reduction at the same concentration. The most plausible reason for dissimilarity between them at higher concentration is the "effective" contact time of products with bacteria. At lower concentration, sphere and fiber products provide almost the same contacting with bacteria, while their contacting actions are quite different at higher concentration. Compared with sphere products, overlapping fiber products with high concentration can construct antibacterial "filter screen", which can effectively prevent bacteria wander arbitrarily, thus can extend retention time of bacteria in the antibacterial circumstances, as a result showing enhanced antibacterial activity. At the concentration higher than 100 mg/mL, sphere products present a somewhat decreased tendency in bacterial reduction. Namely, further increase in concentration of sphere products hinders the antibacterial activity. This can be explained as follows. Although concentration increase of *N*-halamines usually results in enhanced antibacterial efficacy, it can also lead to higher hydrophobicity of the surface, resulting in poor contact with the bacteria and, thus, less efficiency.[40]

Based on the results mentioned above, *N*-halamine polymers with fiber morphology have enhanced antibacterial activity than their corresponding sphere shape products. Because we speculate that the "net-like" fibers have superior capability than the "alone located" spheres. To further verify the exact cause for such an improvement, the zeta potentials of pure PMMA, poly(ADMH-*co*-MMA), *N*-halamine spheres, $fibers_{CEC}$, $fibers_{CCE}$, *E. coli*, and *S. aureus* were analyzed as shown in Figure 12. Pure PMMA shows negative potential, and the introduction of ADMH component into the PMMA polymers has no significant effect on tuning their zeta potentials.[41] Compara-

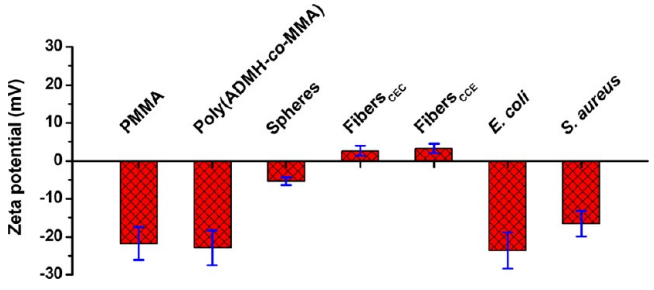

Figure 12. Zeta potential of pure PMMA, poly(ADMH-*co*-MMA), *N*-halamine spheres, *N*-halamine $fibers_{CEC}$, *N*-halamine $fibers_{CCE}$, *E. coli*, and *S. aureus*.

DOI: 10.1021/acsami.5b05429
ACS Appl. Mater. Interfaces 2015, 7, 17516−17526

tively, the chlorination of poly(ADMH-*co*-MMA) can increase their zeta potentials, as a result giving *N*-halamine spheres with higher zeta potentials. The most possible reason is that of the positive charged chlorine (Cl^+) on the surface of *N*-halamines. Unlike PMMA, poly(ADMH-*co*-MMA), and *N*-halamine spheres with negative potentials, both two fibers ($fibers_{CEC}$ and $fibers_{CCE}$) from electrospinning offer positive zeta potentials, which suggests that electrospinning changed the zeta potentials from negative to positive.[42] Such a change is in good agreement with those in the previous reports.[42,43] It is plausible because the high voltage applied for electrospinning might cause the rearrangement of surface charge of the materials, as a result showing positive zeta potential.[43] As for bacteria, both *E. coli* and *S. aureus* carry negative charges, and thus, they can easily adhere to materials carrying positive charges.[44] Therefore, the positive charged fibers can be much closer to bacteria than the negative charged spheres, and in this way, *N*-halamine fibers give enhanced bacteria killing.[45] In general, *N*-halamine fibers have improved antibacterial activity compared with *N*-halamine spheres, which is closely related to their morphology (fiber shapes), surface state (rough surfaces), and surface charge (positive zeta potentials).

CONCLUSIONS

In summary, novel antibacterial agents, *N*-halamine fibers, were controllably fabricated from their sphere morphology precursors by a combined copolymerization−electrospinning−chlorination (CEC) technique. The sphere−fiber transformations were designed logically, and the products were fully characterized by different techniques, namely, SEM, EDS, elemental mapping, FTIR, and ^1H NMR. The effects of reaction conditions on the morphology of the *N*-halamine fibers were systematically evaluated, and the corresponding antibacterial activities were tested using *E. coli* and *S. aureus* as model bacteria. Antibacterial experiments proved that the as-synthesized *N*-halamine fibers possess excellent disinfection behavior toward both bacteria strains. Unexpectedly, *N*-halamine fibers provide obvious enhancement compared with their sphere-shaped precursors, possibly due to their fiber morphology, rough surface, and positive zeta potentials. We believe that this combined CEC technique has great potential in the future for not only antibacterial fields but also other applications.

AUTHOR INFORMATION

Corresponding Author

* E-mail: dongali@imu.edu.cn. Tel.: +86 471 4992982.

Notes

The authors declare no competing financial interest.

ACKNOWLEDGMENTS

This research was supported by the National Natural Science Foundation of China (21304044) and the Program of Higher-level Talents of Inner Mongolia University (30105-125136).

REFERENCES

(1) Miranda, O. R.; Li, X.; Garcia-Gonzalez, L.; Zhu, Z.; Yan, B.; Bunz, U. H. F.; Rotello, V. M. Colorimetric bacteria sensing using a supramolecular enzyme-nanoparticle biosensor. *J. Am. Chem. Soc.* **2011**, *133*, 9650−9653.

(2) Komnatnyy, V. V.; Chiang, W.; Tolker-Nielsen, T.; Givskov, M.; Nielsen, T. E. Bacteria-triggered release of antimicrobial agents. *Angew. Chem., Int. Ed.* **2014**, *53*, 439−441.

(3) Song, J.; Jang, J. Antimicrobial polymer nanostructures: Synthetic route, mechanism of action and perspective. *Adv. Colloid Interface Sci.* **2014**, *203*, 37−50.

(4) Bull, R. J.; Reckhow, D. A.; Li, X.; Humpage, A. R.; Joll, C.; Hrudey, S. E. Potential carcinogenic hazards of non-regulated disinfection by-products: haloquinones, halo-cyclopentene and cyclohexene derivatives, *N*-halamines, halonitriles, and heterocyclic amines. *Toxicology* **2011**, *286*, 1−19.

(5) Cerkez, I.; Worley, S. D.; Broughton, R. M.; Huang, T. S. Rechargeable antimicrobial coatings for poly(lactic acid) nonwoven fabrics. *Polymer* **2013**, *54*, 536−541.

(6) Wu, L.; Liu, A.; Li, Z. Effect of *N*-halamine siloxane precursors on antimicrobial activity and durability of cotton fibers. *Fibers Polym.* **2015**, *16*, 550−559.

(7) Zhang, B.; Jiao, Y.; Kang, Z.; Ma, K.; Ren, X.; Liang, J. Durable antimicrobial cotton fabrics containing stable quaternarized *N*-halamine groups. *Cellulose* **2013**, *20*, 3067−3077.

(8) Kenawy, E. R.; Worley, S. D.; Broughton, R. The chemistry and applications of antimicrobial polymers: a state-of-the-art review. *Biomacromolecules* **2007**, *8*, 1359−1382.

(9) Dong, A.; Zhang, Q.; Wang, T.; Wang, W.; Liu, F.; Gao, G. Immobilization of cyclic *N*-halamine on polystyrene-functionalized silica nanoparticles: synthesis, characterization, and biocidal activity. *J. Phys. Chem. C* **2010**, *114*, 17298−17303.

(10) Lu, X.; Wang, C.; Wei, Y. One-dimensional composite nanomaterials: Synthesis by electrospinning and their applications. *Small* **2009**, *5*, 2349−2370.

(11) Wang, H.; Li, Y.; Sun, L.; Li, Y.; Wang, W.; Wang, S.; Xu, S.; Yang, Q. Electrospun novel bifunctional magnetic-photoluminescent nanofibers based on Fe_2O_3 nanoparticles and europium complex. *J. Colloid Interface Sci.* **2010**, *350*, 396−401.

(12) Miao, Y.; Fan, W.; Chen, D.; Liu, T. High-performance supercapacitors based on hollow polyaniline nanofibers by electrospinning. *ACS Appl. Mater. Interfaces* **2013**, *5*, 4423−4428.

(13) Cavaliere, S.; Subianto, S.; Savych, I.; Jones, D. J.; Rozière, J. Electrospinning: Designed architectures for energy conversion and storage devices. *Energy Environ. Sci.* **2011**, *4*, 4761−4785.

(14) Zhang, C.; Yu, S. Nanoparticles meet electrospinning: Recent advances and future prospects. *Chem. Soc. Rev.* **2014**, *43*, 4423−4448.

(15) Liu, S.; Long, Y.; Huang, Y.; Zhang, H.; He, H.; Sun, B.; Sui, Y.; Xia, L. Solventless electrospinning of ultrathin polycyanoacrylate fibers. *Polym. Chem.* **2013**, *4*, 5696−5700.

(16) Wu, J.; Wang, N.; Zhao, Y.; Jiang, L. Electrospinning of multilevel structured functional micro-/nanofibers and their applications. *J. Mater. Chem. A* **2013**, *1*, 7290−7305.

(17) Kakade, M.; Givens, S.; Gardner, K.; Lee, K. H.; Chase, D. B.; Rabolt, J. F. Electric field induced orientation of polymer chains in macroscopically aligned elctrospun polymer nanofibers. *J. Am. Chem. Soc.* **2007**, *129*, 2777−2782.

(18) Wang, W.; Wang, X.; Yang, Q.; Fei, X.; Sun, M.; Song, Y. A reusable nanofibrous film chemosensor for highly selective and sensitive optical signaling of Cu^{2+} inaqueous media. *Chem. Commun.* **2013**, *49*, 4833−4835.

(19) Tan, K.; Obendorf, S. K. Fabrication and evaluation of ectrospun nanofibrous ntimicrobial nylon 6 membranes. *J. Membr. Sci.* **2007**, *305*, 287−298.

(20) Sun, X.; Zhang, L.; Cao, Z.; Deng, Y.; Liu, L.; Fong, H.; Sun, Y. Electrospun composites nanofiber fabrics containing uniformly dispersed antimicrobial agents as an innovative type of polymeric materials with superior antimicrobial efficacy. *ACS Appl. Mater. Interfaces* **2010**, *2*, 952−956.

(21) Li, R.; Dou, J.; Jiang, Q.; Li, J.; Xie, Z.; Liang, J.; Ren, X. Preparation and antimicrobial activity of *β*-cyclodextrin derivative copolymers/cellulose acetate nanofibers. *Chem. Eng. J.* **2014**, *248*, 264−272.

(22) Sun, Y.; Sun, G. Novel regenerable *N*-halamine polymeric biocides. I. Synthesis, characterization, and antibacterial activity of hydantoin-containing polymers. *J. Appl. Polym. Sci.* **2001**, *80*, 2460−2467.

DOI: 10.1021/acsami.5b05429
ACS Appl. Mater. Interfaces 2015, 7, 17516−17526

(23) Dong, A.; Huang, Z.; Lan, S.; Wang, Q.; Bao, S.; Siriguleng; Zhang, Y.; Gao, G.; Liu, F.; Harnoode, C. *N*-Halamine-decorated polystyrene nanoparticles based on 5-allylbarbituric acid: From controllable fabrication to bactericidal evaluation. *J. Colloid Interface Sci.* **2014**, *413*, 92−99.
(24) Wehling, J.; Dringen, R.; Zare, R. N.; Maas, M.; Rezwan, K. Bactericidal Activity of Partially Oxidized Nanodiamonds. *ACS Nano* **2014**, *8*, 6475−6483.
(25) Yu, H.; Zhang, X.; Zhang, Y.; Liu, J.; Zhang, H. Development of a hydrophilic PES ultrafiltration membrane containing SiO_2@*N*-halamine nanoparticles with both organic antifouling and antibacterial properties. *Desalination* **2013**, *326*, 69−76.
(26) Jang, J.; Kim, Y. Fabrication of monodisperse silica-polymer core-shell nanoparticles with excellent antimicrobial efficacy. *Chem. Commun.* **2008**, 4016−4018.
(27) Gutman, O.; Natan, M.; Banin, E.; Margel, S. Characterization and antibacterial properties of *N*-halamine-derivatized cross-linked polymethacrylamide nanoparticles. *Biomaterials* **2014**, *35*, 5079−5087.
(28) Chen, Z.; Sun, Y. *N*-Halamine-based antimicrobial additives for polymers: Preparation, characterization, and antimicrobial activity. *Ind. Eng. Chem. Res.* **2006**, *45*, 2634−2640.
(29) Li, C.; Xue, L.; Cai, Q.; Bao, S.; Zhao, T.; Xiao, L.; Gao, G.; Harnoode, C.; Dong, A. Design, synthesis and biocidal effect of novel amine *N*-halamine microspheres based on 2,2,6,6-tetramethyl-4-piperidinol as promising antibacterial agents. *RSC Adv.* **2014**, *4*, 47853−47864.
(30) Wang, W.; Li, Y.; Sun, M.; Zhou, C.; Zhang, Y.; Li, Y.; Yang, Q. Colorimetric and fluorescent nanofibrous film as a chemosensor for Hg^{2+} in aqueous solution prepared by electrospinning and host-guest interaction. *Chem. Commun.* **2012**, *48*, 6040−6042.
(31) Yan, X.; Jie, Z.; Zhao, L.; Yang, H.; Yang, S.; Liang, J. High-efficacy antibacterial polymeric micro/nano particles with *N*-halamine functional groups. *Chem. Eng. J.* **2014**, *254*, 30−38.
(32) Cai, Q.; Bao, S.; Zhao, Y.; Xiao, L.; Gao, G.; Chokto, H.; Dong, A. Tailored synthesis of amine *N*-halamine copolymerized polystyrene with capability of killing bacteria. *J. Colloid Interface Sci.* **2015**, *444*, 1−9.
(33) Kumar, A. S.; Sornambikai, S.; Deepika, L.; Zen, J. Highly selective immobilization of amoxicillin antibiotic on carbon nanotube modified electrodes and its antibacterial activity. *J. Mater. Chem.* **2010**, *20*, 10152−10158.
(34) Cui, J.; Hu, C.; Yang, Y.; Wu, Y.; Yang, L.; Wang, Y.; Liu, Y. Facile fabrication of carbonaceous nanospheres loaded with silver nanoparticles as antibacterial materials. *J. Mater. Chem.* **2012**, *22*, 8121−8126.
(35) Li, C.; Hou, J.; Huang, Z.; Zhao, T.; Xiao, L.; Gao, G.; Harnoode, C.; Dong, A. Assessment of 2,2,6,6-tetramethyl-4-piperidinol-based amine *N*-halamine-labeled silica nanoparticles as potent antibiotics for deactivating bacteria. *Colloids Surf., B* **2015**, *126*, 106−114.
(36) Bogdanovic, U.; Vodnik, V.; Mitric, M.; Dimitrijevic, S.; Skapin, S. D.; Zunic, V.; Budimir, M.; Stoiljkovic, M. Nanomaterial with high antimicrobial efficacy-copper/polyaniline nanocomposite. *ACS Appl. Mater. Interfaces* **2015**, *7*, 1955−1966.
(37) Li, S.; Wang, Z.; Wei, Y.; Wu, C.; Gao, S.; Jiang, H.; Zhao, X.; Yan, H.; Wang, X. Antimicrobial activity of a ferrocene-substituted carborane derivative targeting multidrug-resistant infection. *Biomaterials* **2013**, *34*, 902−911.
(38) Liu, Y.; Li, J.; Cheng, X.; Ren, X.; Huang, T. S. Self-assembled antibacterial coating by *N*-halamine polyelectrolytes on a cellulose substrate. *J. Mater. Chem. B* **2015**, *3*, 1446−1454.
(39) Sun, Y.; Zhang, Y.; Xia, Y.; Fan, T.; Xue, M.; Bulgan; Enkhbayar; Harnoode, C.; Dong, A. Evaluation of physicochemical properties and bactericidal activity of efficient Chemical Germicidal Water (CGW). *LWT-Food Sci. Technol.* **2014**, *59*, 1068−1074.
(40) Dong, A.; Sun, Y.; Lan, S.; Wang, Q.; Cai, Q.; Qi, X.; Zhang, Y.; Gao, G.; Liu, F.; Harnoode, C. Barbituric acid-based magnetic *N*-halamine nanoparticles as recyclable antibacterial agents. *ACS Appl. Mater. Interfaces* **2013**, *5*, 8125−8133.
(41) Valerio, A.; Nicoletti, G.; Cipolatti, E. P.; Ninow, J. L.; Araujo, P. H. H.; Sayer, C.; de Oliveira, D. Kinetic study of *Candida antarctica* Lipase B immobilization using poly(methyl methacrylate) nanoparticles obtained by miniemulsion polymerization as support. *Appl. Biochem. Biotechnol.* **2015**, *175*, 2961−2971.
(42) Okutan, N.; Terzi, P.; Altay, F. Affecting parameters on electrospinning process and characterization of electrospun gelatin nanofibers. *Food Hydrocolloids* **2014**, *39*, 19−26.
(43) Esfahani, H.; Prabhakaran, M. P.; Salahi, E.; Tayebifard, A.; Keyanpour-Rad, M.; Rahimipour, M.; Ramakrishna, S. Protein adsorption on electrospun zinc doped hydroxyapatite containing nylon 6 membrane: Kinetics and isotherm. *J. Colloid Interface Sci.* **2015**, *443*, 143−152.
(44) Tian, Y.; Qi, J.; Zhang, W.; Cai, Q.; Jiang, X. Facile, one-pot synthesis, and antibacterial activity of mesoporous silica nanoparticles decorated with well-dispersed silver nanoparticles. *ACS Appl. Mater. Interfaces* **2014**, *6*, 12038−12045.
(45) Pan, X.; Wang, Y.; Chen, Z.; Pan, D.; Cheng, Y.; Liu, Z.; Lin, Z.; Guan, X. Investigation of antibacterial activity and related mechanism of a series of nano-$Mg(OH)_2$. *ACS Appl. Mater. Interfaces* **2013**, *5*, 1137−1142.

DOI: 10.1021/acsami.5b05429
ACS Appl. Mater. Interfaces 2015, 7, 17516−17526